Advanced Steel Construction – Vol. 20 No. 3 (2024) 208–221
DOI:10.18057/IJASC.2024.20.3.1

SEISMIC FRAGILITY ANALYSIS OF STEEL FRAMES WITH FULLY-BOLTED CORE TUBE JOINTS

Yun-Peng Chu, Xue-Qin Chen *, Yan Zhong and Hai-Chuan Zhang

School of Civil Engineering and Architecture, Southwest University of Science and Technology, Mianyang 621010, China
** (Corresponding author: E-mail: chenxueqinswust@qq.com)*

ABSTRACT

In this paper, the joint parameters derived from testing the new fully-bolted core tube beam-column joint were utilized in the finite element analysis of the complete frame structure. The static elastic-plastic time-history analysis of 8, 12, 16, and 20-story steel frames with the braces was carried out. By comparing the maximum inter-layer displacement angles in the X and Y directions when the frame yielded, the rationality of the brace arrangement and the applicability of the new fully-bolted core tube beam-column joints in the multi-story and high-rise steel frames were confirmed. After dividing the range of damage values for the steel frame with the new fully-bolted core tube beam-column joint, the seismic fragility and collapse resistance of the steel frame with the new fully-bolted core tube beam-column joint of different stories were analyzed. The results show that it is important to note that when the number of stories is low, the probability of each stage of the structure being exceeded is high. However, as the number of stories increases, the impact on the probability of the structure being exceeded gradually decreases. Under the action of a large earthquake peak acceleration, the exceedance probability based on a two-parameter damage index is higher than that based on a single-parameter damage index. This indicates that during the large deformation stage of the structure, the influence of cumulative damage on the evaluation of structural performance cannot be ignored. The steel frame of multi-story and high-rise buildings with new joints may be in a serious damage stage under rare earthquakes, and it is possible to collapse under the action of great earthquakes. In addition, the ACMR value of the structure under the action of rare earthquakes meets the evaluation criteria, while the ACMR value under the action of great earthquakes does not meet the requirements. Therefore, in practical engineering, it is necessary to take seismic strengthening measures to ensure that the structure has sufficient safety reserves against collapse during earthquakes.

ARTICLE HISTORY

Received: 31 August 2023
Revised: 18 March 2024
Accepted: 3 April 2024

KEYWORDS

Fully bolted joint;
Layered assembly steel frame;
Multi-story and high-rise steel frames;
Fragility analysis

1. Introduction

The layered assembled steel frame structure has received extensive attention because the individual components of the structure can be extensively prefabricated in the factory, leading to a more conducive environment for achieving efficient and rapid assembly goals. With the development of society and economy, multi-story and high-rise buildings have gradually become an important carrier of urban economic activities. However, the force situation of the multi-story and high-rise steel frame joint during earthquake is quite complex. Therefore, it is necessary to make a reasonable seismic evaluation of the seismic performance of multi-story and high-rise layered assembled steel frame.

Following the Northridge earthquake and the Osaka earthquake, fragility damage was observed in a majority of the conventional steel frame beam-column joints, prompting numerous scholars to initiate research on enhancing welded joints [1–3]. There is still a risk of weld fracture, even though the enhanced joints show excellent seismic performance. As a result, researchers have gradually advanced the concept of fully bolted joints. Using fully bolted joints can significantly increase the ductility, plastic deformation and energy dissipation capacities of the joint, while also reducing seismic damage from bolt slippage.

Based on this, Shahidi et al. [4] studied the influence of the bolt arrangement on the seismic performance of ConXL joints by numerical simulation. The results show that when the bolt is close to the outer edge of the joint plate, the axial stress of the bolt rod is very large. The closer the bolt is to the flange of the beam, the shear of the bolt rod is generated due to the increase of the slip of the end plate of the beam. The seismic performance of the joint with bolts installed in the middle of the gusset plate is good, and the joint with two rows of bolts on each gusset plate has better seismic performance than the joint with one row of bolts. Lee et al. [5] proposed a modular joint with brace, in which the beams and columns are connected by welding and the modules are connected by connecting plates. The test results show that this joint has good seismic performance. Wang et al. [6] conducted low cyclic loading tests on square steel tube column and H-shaped steel beam joints connected with through bolts. The results show that the seismic performance of the joints with such bolt is better, and it is pointed out that for the unfilled steel tube column, the column wall will have symmetrical concave buckling phenomenon. Hosseini et al. [7] proposed a ring-hoop joint. Through finite element analysis of 18 models with this joint, the optimal design parameters of the joint were obtained. Compared with the short connecting plate, using a longer connecting plate at the beam end to connect to the gusset plate can achieve better joint performance. Liu et al. [8-10] developed a a modular beam-column bolt joint. Their tests demonstrated that the joint has excellent seismic performance.

Seismic fragility is essential for evaluating the seismic reliability of structures, improving their seismic design, preventing earthquake disasters, performing follow-up maintenance, and strengthening structures after an earthquake. Lv et al. [11] used the Incremental Dynamic Analysis (IDA) to evaluate the seismic fragility of a non-standard high-rise building. They determine the probability that a structure will surpass its limit state. The results show it can be used to determine the damage and loss of structures in earthquakes. Pushover and IDA were performed on steel frames by Fanaie et al. [12] and Mohebi [13] et al. They classified the limit states based on the damage index as a performance level indicator. The limit state correction coefficients of the structure were finally got. Accounting for random ground motion and structure uncertainty, Pandikkadavath et al [14] analyzed the seismic fragility of the structure. Correction coefficients for the response discounting parameters for the seismic design of enhanced structures were obtained. The collapse probability and anti-collapse reserve coefficient of the structure were quantitatively evaluated by Wang et al. [15] through IDA analysis of a steel frame supported by multi-layer beams with varying joint stiffness. Li et al. [16] used the seismic risk theory to conduct probabilistic seismic demand analysis for structures. The probability of structural earthquake occurrence and the characteristics of structural seismic response are determined.

Currently, the traditional column-through-structure is the main focus of research efforts on the seismic fragility of steel structures. However, there is a lack of extensive research on steel frames with layered assembled connections. Today, the fully bolted joint design concept is more sophisticated [17–20], but there are problems that complex joints are not easy to quickly assemble and simple joints don't have good seismic performance. To address these issues, A novel fully-bolted core tube beam-column joint was proposed and subsequently subjected to quasi-static tests. In order to explore the applicability and feasibility of this kind of joints applied to the middle and high-rise frame, the joint test parameters were introduced into the whole frame structure. Four braced steel frame models with the new joint with total stories of 8, 12, 16, and 20 were established by SAP2000 for static elastic-plastic time history analysis and incremental dynamic analysis. The damage value range of the frame with the new joint was re-divided. The plastic angle distribution and collapse resistance of the frame models with the new joint were obtained. The feasibility and effectiveness of the new joint applied to the multi-story and high-rise steel frame have been systematically evaluated, which serves as a reference for evaluating the seismic performance of similar structures.

2. Joint test and simplified mechanical model

2.1. Joint test

The seismic performance of the entire structure may be affected by the loading characteristics of the connections between the steel frame beams and columns, as they are the main transmission part of the structure. A new fully bolted core tube joint (XJD) is designed based on the concept of energy dissipation-seismic reduction. The traditional column-through joint (CJD) is used as the control group, and the quasi-static test is carried out on the new and traditional joint [21]. CJD (Fig. 1a) was the commonly used beam-column joint. XJD consists three components: a square steel tube column, an H-shaped beam and a core tube joint.

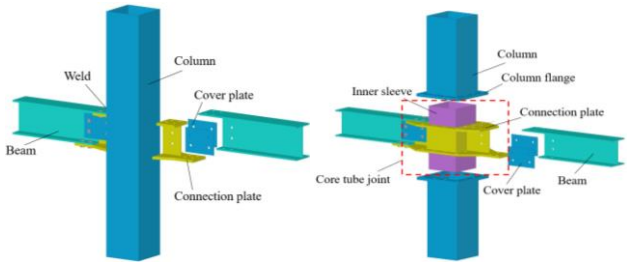

(a) (b)

Fig. 1 3D diagram of test joints. (a) CJD. (b) XJD

The CJD and XJD are both constructed as steel frame beam-column joints. The primary difference between two types of joints is XJD by practice. Unlike the CJD, it disconnects the column at the floor connection and establishes connections between the upper and lower columns and beams using a connecting plate located on the column base within the joint domain. This innovative design allows for a layered assembly technique to be implemented. The CJD design features that the column is through, and is connected by setting a connecting plate welded to the column wall at the beam-column connection. This design carries the risk of weld cracking during an earthquake. Through a comparison of the test results from the two kinds of joints, the XJD's enhanced seismic performance can be better demonstrated. Fig. 2 displays the test-loading device and the layout of the site.

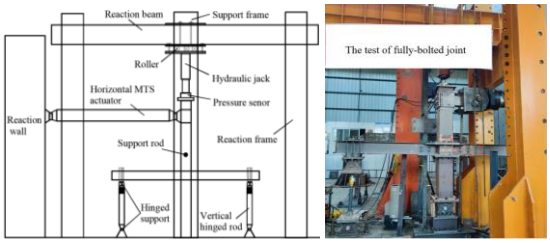

(a) (b)

Fig. 2 The test-loading device and the layout of the site. (a) Test-loading device. (b) Layout of the site

The test results showed that in comparison to the CJD, the XJD exhibited a 471.39% increase in total energy consumption, a 27.52% increase in ductility coefficient, a 20.35% increase in yield load, and a 38.56% increase in ultimate load. It could be seen that the XJD's seismic performance was obviously better than the CJD.

2.2. Simplified mechanical analysis model

Joint differences between steel frame and reinforced concrete frame structures These joints are not fully bonded. A welded joint is called a rigid joint, and a bolted joint is called a flexible joint. The research suggests that because of the still existing some rotational stiffness in welded or bolted joints, they cannot be easily classified as either rigid or flexible joints. In this paper, the Bjorhovde [22] and Eurocode3 [23] procedures are used to determine the XJD's and CJD's properties. The M_{ratio} and θ_{ratio} are calculated and presented in Fig. 3.

It can be seen from Fig. 3 that the Eurocode3 method has a larger range. The M_{ratio}-θ_{ratio} curves for XJD and CJD are fall within the range of semi-rigid joints based on the Eurocode3 method. Based on the Bjorhovde method, CJD's M_{ratio}-θ_{ratio} curve is classified as semi-rigid. Similarly, the semi-rigid classification also applies to the first half of XJD's M_{ratio}-θ_{ratio} curve. The increase in the angle of rotation of the two joints may be due to bolt slippage or weld cracks, resulting in a gradual increase in the bending moment at the end of the beam. This causes the joints to exhibit a semi-rigid joint performance. The XJD's M_{ratio}-θ_{ratio} curve keeps to increasing, indicating that the bending capacity is excellent. The curve of M_{ratio}-θ_{ratio} in CJD initially increases and then decreases. It can be caused by the reduction in bending capacity during plastic deformation due to weld cracking and column wall buckling. According to Bjorhovde's method, the XJD will remain in the semi-rigid region of the joint during both the plastic and the elastic-plastic deformation stages, although it exhibits rigid joint properties in the later stages of loading due to the continued plastic deformation. According to the two methods for the classification of joint properties, XJD and CJD are considered to be semi-rigid joints.

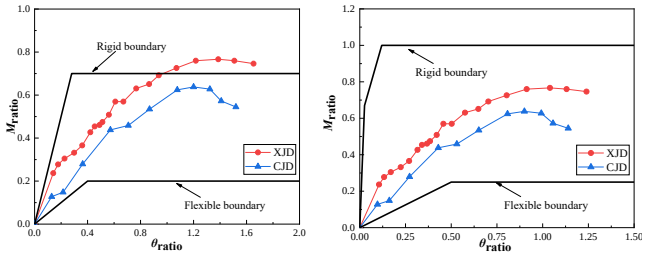

（a）Bjorhovde method （b）Eurocode3 method

Fig. 3 Connection property calculation results

It has been discovered that both XJD and CJD are types of semi-rigid joints. On the basis of the code GB50017-2017 [24], the rotational angle of the beam-column semi-rigid connection will change when subjected to bending moment, but its rotational stiffness is restrained. To simulate the semi-rigid joint using the nonlinear connector, it is essential to choose a suitable M-θ model. The M-θ curve of the tested joints was subjected to dimensionless processing, taking into account the impact of specimen parameters. It was then fitted using the trilinear model. The equation used for fitting is presented in Table 1. The comparison between the normalized joint test M-θ curve and the fitted M-θ curve is shown in Fig. 4. Based on Fig. 4, it is clear that the M-θ curve closely matches the curve obtained from the test when fitted using the trilinear model. This makes it appropriate for simplifying joint calculations.

Table 1
Tri-linear fitting equations for normalized M-θ curves of joints

Folded line segment	XJD	CJD
OA	$M/M_{max} = 1.838\,\theta/\theta_{max}$	$M/M_{max} = 1.363\,\theta/\theta_{max}$
AB	$M/M_{max} = 0.385 + 0.624\,\theta/\theta_{max}$	$M/M_{max} = 0.292 + 0.689\,\theta/\theta_{max}$
BC	$M/M_{max} = 1.061$	$M/M_{max} = 1.722 - 0.731\,\theta/\theta_{max}$

Note: M_{max} is the bending moment corresponding to the ultimate load, and θ_{max} is the rotation angle corresponding to the ultimate load.

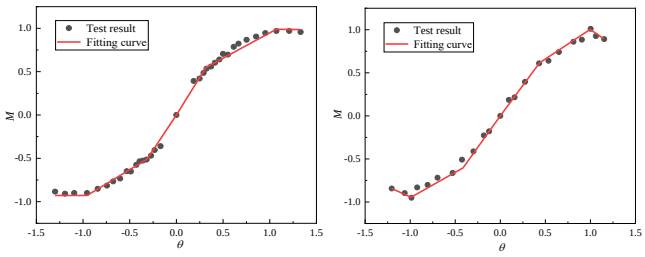

(a) (b)

Fig. 4 Compare Joint Test and Fitted *M-θ* Curve. (a) XJD. (b) CJD

The semi-rigid connection is simulated using the kinematic restoring force model, and the hysteresis model is shown in Fig. 5. Using the method described above, the FEA models for the new joint and the traditional joint are created in SAP2000. The simplified analysis model is illustrated in Fig. 6.

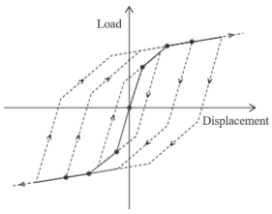

Fig. 5 Kinematic hysteretic model

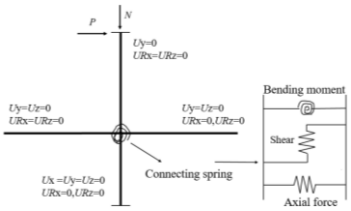

Fig. 6 Simplified mechanical analysis model

In simplified joint analysis, the beam is represented as a bar element connected to two zero-length rotational springs at the bar ends. The axial and shear deformations of the end torsion springs are not considered, and only their bending deformations are taken into account. Rigid blocks were attached to both ends of the column. These were used to apply loads or set boundary conditions. Both an axial load and a cyclic load have been subjected to the top of the column. The boundary conditions of the numerical model were identical to those of the test joint. At the bottom of the column, three directions of translation were limited, while at the top of the column, translation in the Y direction was limited. The beam ends were restrained to avoid out-of-plane instability in all directions besides the X-direction. The characteristic points in the fitted M-θ curve are defined within the kinematic restoring force model's corner spring unit. The column is subjected to a concentrated load *N* and a reciprocating load *P*. Based on the test conditions, the model constraints are set. The XJD initial torsional rigidity (K_1) link spring is 3.4×10^4 kN·m/rad. The XJD initial torsional rigidity (K_2) link spring is is 3.0×10^4 kN·m/rad. Fig.7 compares the results obtained using the simplified model and the joint test.

Based on Fig. 7, it is evident that the *M-θ* curve of the joint between the test and the simplified model exhibits a strong correlation. XJD and CJD had an ultimate bending capacity of 200.59 kN·m and 152.89 kN·m, respectively, according to the test results. Using the simplified model, the ultimate bending capacities of XJD and CJD were calculated as 213.68kN·m and 139.28kN·m, respectively. The errors between the test results and the simplified model calculation results were 6.53% and -8.9% respectively, both percentages were below 15%. This demonstrates that the simplified model is highly accurate for joint simulation and can be used for further analysis of the overall model.

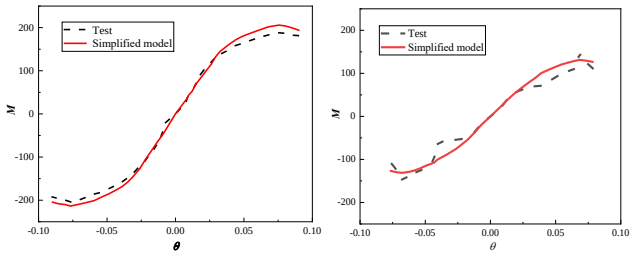

(a) (b)

Fig. 7 Compare simplified model calculations and test results. (a) XJD. (b) CJD

3. Static elastic-plastic time-history analysis

3.1. Design basic parameters

The steel frame structures were situated in an area characterized by a seismic intensity of 8. Design basic ground motion acceleration is 0.2g. Site classification is II, Site characteristic period (Tg) is 0.40s. Site roughness is class C. The design considers a floor dead load of 4.0 kN/m^2 and a live load of 2.0 kN/m^2. The beam was assigned a line load of 10 kN/m. The snow load on the roof was taken as 0.5 kN/m^2. The wind load was taken as 0.3 kN/m^2.

3.2. Finite element Model

Four steel frame structures are designed by PKPM as the calculation models, of which the stories are 8, 12, 16, and 20, respectively. In combination with Reference [25], the inverted V-shaped center brace is arranged in the steel frame structures. The size of the structural members is shown in Tables 2 to 5. The actual layout is shown in Fig. 8. Subsequently, the models are established by SAP2000, with the joint parameters referencing the simplified mechanical model mentioned earlier. The foundation is consolidated. The spring element was placed at the fracture of the beam-column joint. The initial stiffness and *M-θ* curve eigenvalues of both the XJD and CJD were defined into the spring element. The load cases were set as gravity load conditions and pushover load conditions. Nonlinear Static Analysis was selected as the type of structural analysis. The geometric nonlinearity is set to *P-Δ* nonlinearity. The initial condition of the pushover load case is relay nonlinear. The loading option is displacement control. The displacement type is selected to monitor the displacement, and the displacement target value is 0.04 times the building height. The coefficients of plastic hinge setting from the end points of the structural components were 0.1 and 0.9, respectively. *PMM* hinge was used for columns, *M* hinge was used for beams and *P* hinge was used for braces.

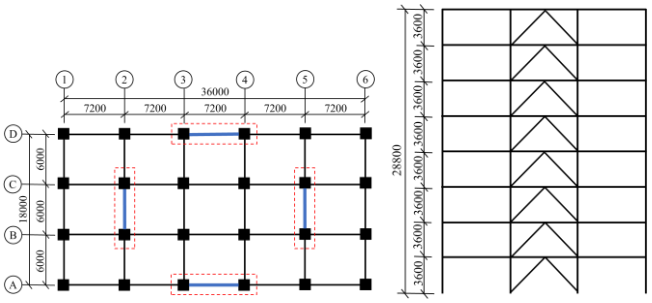

(a) (b)

Fig. 8 Steel frame layout. (a) Plan layout. (b) Elevation layout

Table 2
8-story component size parameters

Model	Material	Components	Section
8-story	Q235	Corner column	1~8 stories: □500×18
		Middle column	1~8 stories: □550×30
		Beam	1~8 stories: H400×200×8×13
		Brace	1~8 stories: H175×90×5×8

Table 3
12-story component size parameters.

Model	Material	Components	Section
12-story	Q355	Corner column	1~6 stories: □500×18; 7~12 stories: □500×16
		Middle column	1~3 stories: □700×30; 4~6 stories: □650×30; 7~12 stories: □600×26
		Beam	1~6 stories: H600×200×10×15; 7~12 stories: H600×200×10×15
		Brace	1~12 stories: H300×150×6.5×9

Table 4
16-story component size parameters

Model	Material	Components	Section
16-story	Q355	Corner column	1~8 stories: □500×18； 9~16 stories: □500×16
		Middle column	1~3 stories: □650×30； 4~6 stories: □600×28; 7~9 stories: □500×30 10~12 stories: □500×28; 13~16 stories: □500×26
		Beam	1~8 stories: H500×200×9×14; 9~16 stories: H450×200×9×14
		Brace	1~16 stories: H350×175×7×11

Table 5
20-story component size parameters

Model	Material	Components	Section
20-story	Q355	Corner column	1~5 stories: □500×30; 6~10 stories: □500×30; 11~20 stories: □500×24
		Middle column	1~3 stories: □850×30; 4~6 stories: □750×30; 7~9 stories: □650×30; 10~15 stories: □500×26; 16~18 stories: □500×22; 19~20 stories: □500×18
		Beam	1~5 stories: H500×200×9×14; 6~10 stories: H450×200×9×14; 11~15 stories: H500×150×10×16; 16~20 stories: H450×150×9×14
		Brace	1~20 stories: H400×200×8×13

3.3. Distribution of plastic hinges

The distribution of the interlayer displacement angle and the plastic hinge for the four models at different stages are shown in Figs. 9 to 13. Specifically, (a) indicates the plastic hinge first appears in the brace. (b) indicates the plastic hinge first appears in the beam. (c) indicates the plastic hinge first appears in the column. (d) indicates the plastic hinge distribution of the structure when the maximum inter-layer displacement angle reaches 1/50.

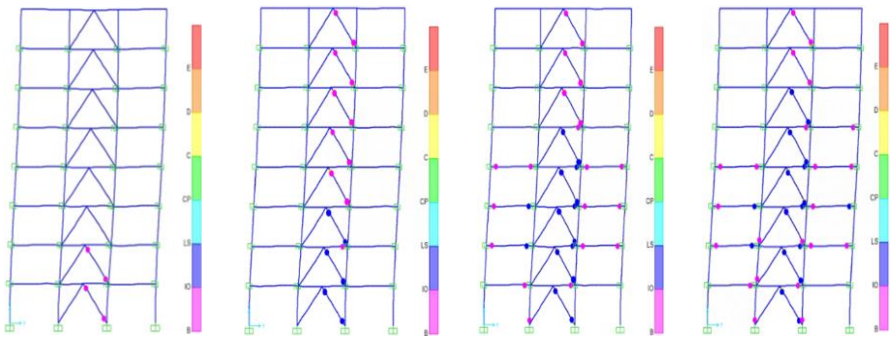

(a) (b) (c) (d)

Fig. 9 8-story

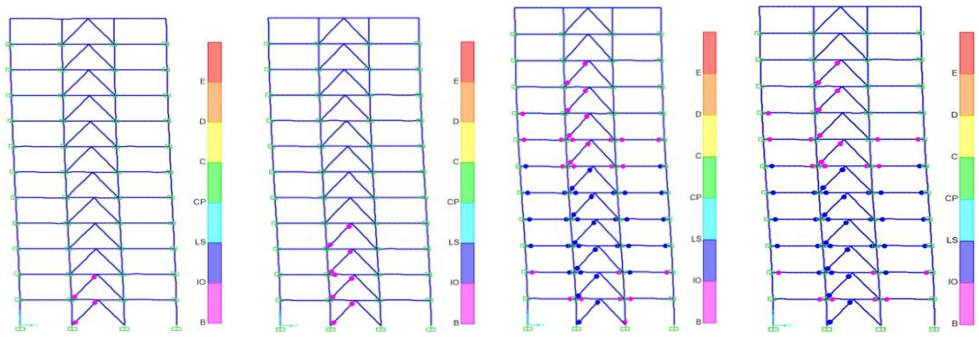

(a) (b) (c) (d)

Fig. 10 12-story

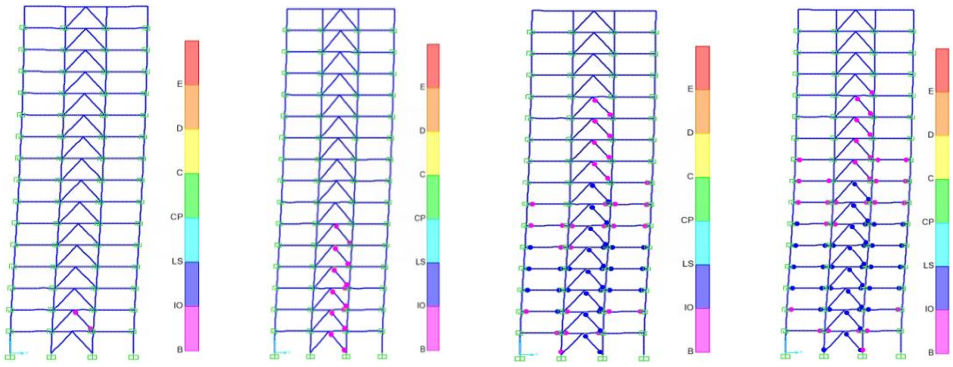

(a) (b) (c) (d)

Fig. 11 16-story

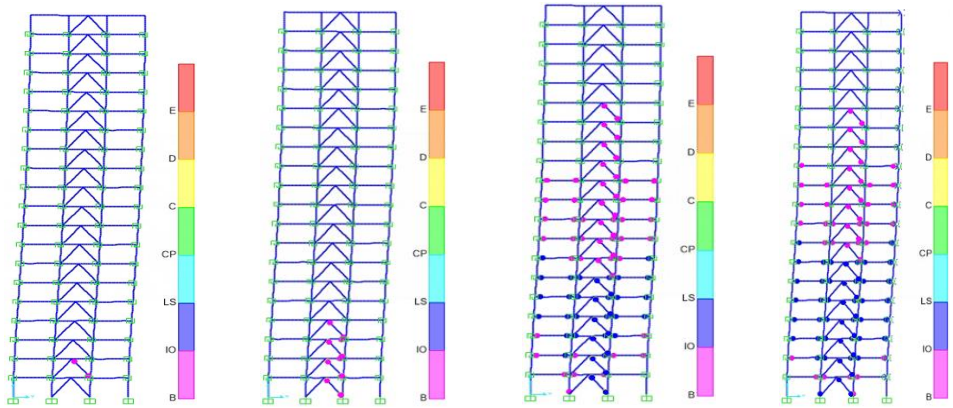

(a) (b) (c) (d)

Fig. 12 20-story

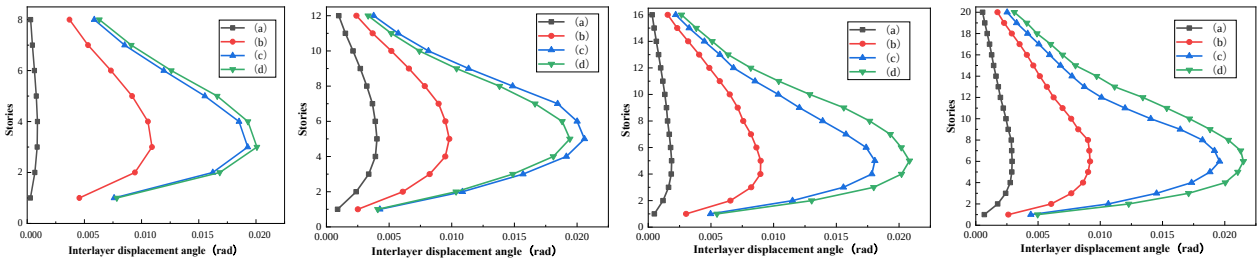

(a) (b) (c) (d)

Fig. 13 Distribution of interlayer displacement angle. (a) 8-story. (b) 12-story. (c) 16-story. (d) 20-story

The distribution of inter-layer displacement angle is presented in Fig. 13. According to the analysis of the distribution of plastic hinge and inter-layer displacement angle in each stage of the steel frame structure, the plastic hinges first appear in the brace, then in the beam, and finally begins to develop on the column. In addition, before the interlayer displacement angle reaches 0.02 rad, most of the braces and beams have entered the stage of plastic deformation development, and the steel frame presents the fortification requirement of "strong column and weak beam" before the failure of the braces and beams, which conforms to the seismic design concept of the steel frame structure. Moreover, when the inter-layer displacement angle reaches 0.02 rad, only the 1 to 3 story middle columns of the 8-story structure have plastic hinges, while the 16-story and 20-story structures show plastic hinges only in the middle columns of the bottom story and all the columns of the 12-story structure are still in the elastic deformation stage. These mean that four models are in accordance with the idea of “capacity design”. The selection of structural components is appropriate and the arrangement is reasonable. It also means that it is conservative to use the elastic-plastic inter-layer displacement angle of 1/50 as the collapse criterion of the steel frame structure with the new jointed.

3.4. Pushover curves

The response spectrum in SAP2000 is the ATC-40 [26] response spectrum. The parameters C_A and C_V need to be changed to make the structure calculation conform to the Chinese code. C_A and C_V can be calculated by Eq. (1) and Eq. (2), respectively.

$$\eta_2\alpha_{max} = 2.5C_A \quad (1)$$

$$T_g = T_s = C_V / 2.5C_A \quad (2)$$

where, $\eta_2\alpha_{max}$ is the maximum value of the horizontal seismic influence coefficient. The site characteristic period T_g is 0.4 s. For an 8-degree frequent earthquake, $\eta_2\alpha_{max}$ = 0.16, and C_A = 0.064, C_V = 0.064 can be obtained through calculation. For an 8-degree rare earthquake, $\eta_2\alpha_{max}$ = 0.9, and C_A = 0.36, C_V = 0.36 can be obtained through calculation.

In the pushover analysis results, the top displacement, spectral displacement, base shear and spectral acceleration at the performance point can be directly viewed to evaluate the seismic performance of the structure. as shown in Fig. 14. The performance point is located at the intersection of the capability spectrum curve and the demand spectrum curve in the same coordinate system. The performance point can be expressed by spectral displacement and spectral acceleration, and the top displacement and base shear at the performance point can be further obtained by Eq. (3) and Eq. (4).

$$V = \alpha_n G S_a \quad (3)$$

$$D = \gamma_n X_n S_d \quad (4)$$

Where α_n is the mass participation coefficient, γ_n is the participation coefficient, and X_n is the vertex amplitude. Because the high-rise steel frame structure is generally dominated by the first vibration mode during the earthquake, only the α_n, γ_n and X_n under the first vibration mode is taken.

When the displacement demand of the structure under the seismic fortification level is less than the structure's actual seismic displacement response, The point where the capacity spectrum and demand spectrum curves intersect will be visible, indicating that the structure is considered to be safe and reliable. Conversely, if the displacement demand exceeds the actual seismic displacement response of the structure, resulting in no intersection between the two curves, the structural performance point does not exist, suggesting that the structure is not safe and reliable at this time. Its seismic performance does not meet the basic requirements and the seismic fortification goals. In such cases, it becomes necessary to either redesign or reinforce the structure.

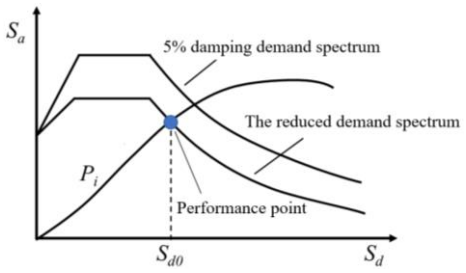

Fig. 14 Structural performance points

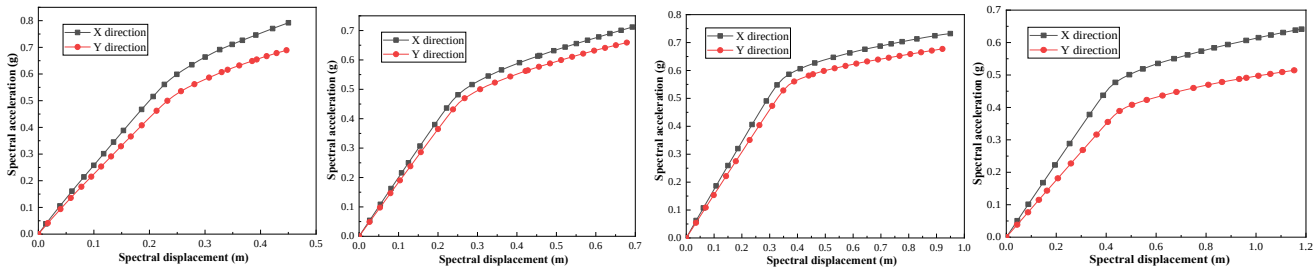

(a) (b) (c) (d)

Fig. 15 Capacity spectrum curve. (a) 8-story. (b) 12-story. (c) 16-story. (d) 20-story

From Fig. 15, it can be seen that under the action of frequent and rare earthquakes, each model has performance points in the X and Y directions. It means that the structure meets the requirements of seismic fortification and is in the safe state. Additionally, the higher the structural stiffness, the lower the ductility and performance level. Under the action of earthquake, as the number of stories increases, the spectral acceleration at the performance point decreases while the spectral displacement increases.

Table 6
Spectral acceleration and spectral displacement (performance points)

Stories		X direction		Y direction	
		Spectral acceleration /g	Spectral displacement /mm	Spectral acceleration /g	Spectral displacement /mm
Frequent earthquake	8	0.071	32.27	0.078	24.96
	12	0.066	33.45	0.070	25.16
	16	0.062	47.00	0.063	41.01
	20	0.059	58.40	0.060	51.18
Rare earthquake	8	0.461	184.03	0.463	161.56
	12	0.381	187.23	0.395	162.95
	16	0.353	283.50	0.361	229.73
	20	0.332	327.42	0.352	286.73

Table 6 shows that under the action of frequent earthquakes, the X-direction spectral displacement of 8-story, 12-story, 16-story, and 20-story models is 29.29%, 32.95%, 14.61%, and 13.91% higher than that of Y-direction, respectively. Similarly, Under the rare earthquakes, the X-direction spectral displacement of 8-story, 12-story, 16-story, and 20-story models is 13.91%, 14.90%, 23.41%, and 14.19% higher than that of Y-direction, respectively. The vibration characteristics of each model in the X direction are larger than those in the Y direction. However, the small difference in the spectral displacement between the two directions, which means that the mass distribution of the structure in the X and Y directions is uniform.

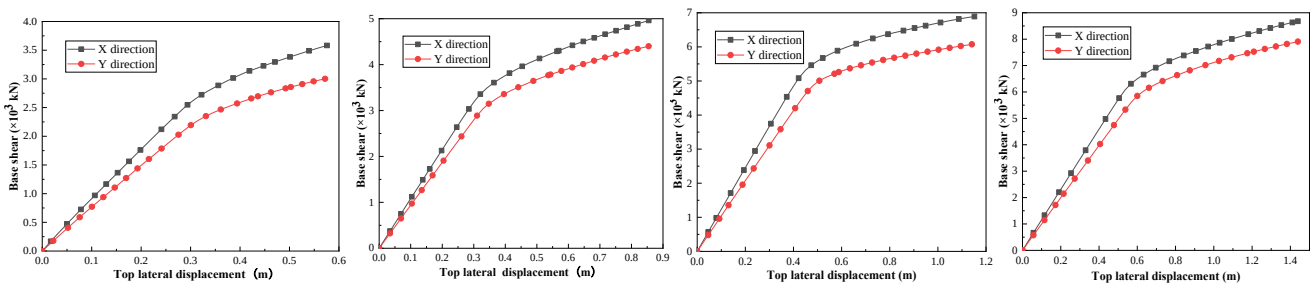

(a) (b) (c) (d)

Fig. 16 Base shear and top lateral displacement curve. (a) 8-story. (b) 12-story. (c) 16-story. (d) 20-story

Fig.15 shows the base shear-top lateral displacement curve of the model. The corresponding top displacement and base shear of the structural performance points provided in Table 7. Notably, all the curves have obvious inflection points. The X-direction base shear of each model is greater than the Y-direction base shear due to the enhanced X-direction lateral stiffness resulting from the central brace. As the number of structural stories increases, the top lateral displacement and base shear also increase. At the performance point of the structure, the base shear in the Y direction is larger than that in the X direction, while the top lateral displacement in the Y direction is smaller than that in the X direction. This indicates that the vibration characteristics of the structure in the Y-direction are smaller than those in the X-direction during the earthquakes.

Table 7
Base shear and top lateral displacement (performance point)

Stories		X direction		Y direction	
		Top lateral displacement /mm	Base shear /kN	Top lateral displacement /mm	Base shear /kN
Frequent earthquake	8	41.99	292.33	35.08	345.73
	12	43.61	341.37	37.41	486.62
	16	61.83	552.07	52.98	765.24
	20	76.86	641.06	66.24	922.61
Rare earthquake	8	238.54	1570.08	209.41	2085.79
	12	244.26	1901.26	209.05	2694.82
	16	347.02	3076.24	297.10	4242.52
	20	433.13	3583.59	373.26	5141.77

According to Table 7, under the action of frequent earthquakes, the top lateral displacement in the X-direction of the 8-story, 12-story, 16-story, and 20-story models is 16.46%, 14.22%, 14.31%, and 13.82% higher than those in the Y-direction, respectively. Under the action of rare earthquakes, the top lateral displacement in the X-direction of the 8-story, 12-story, 16-story, and 20-story models is 12.21%, 14.41%, 14.38%, and 13.82% higher than the top lateral displacement in the Y-direction, respectively. Thus, there is not a significant difference in the lateral displacement between the two directions of the structure under the action of frequent and rare earthquakes.

3.5. Yield displacement angle

The double broken line energy equal area method can be employed to determine the yield point of a structure if the load-displacement curve obtained from pushover analysis does not exhibit a clear yield point. The theoretical model for this method is shown in Fig. 17. The yield point of the structure is defined based on two calculation principles. Firstly, the deformation should be consistent with the energy dissipation, meaning that the area enclosed by the curve is equal to the area enclosed by the double broken line ($S_{OB} = S_{OABE}$). Secondly, the double broken line and the curve are infinitely approximated, and the value that satisfies $m = S_1 + S_2 + S_3$ is minimized. The yield point of the structure is the intersection point C when the above principles are satisfied.

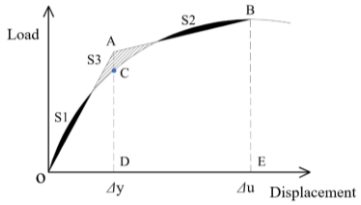

Fig. 17 Double broken line energy equal area method

Except for the 8-story model, the other models have obvious points of contraflexure, i.e., the 12-story, 16-story, and 20-story models all have structural yield points, according to the structural base shear and top lateral displacement curves in Fig. 16. Thus, the method described above is utilized to identify the yield point of the 8-story model. The top lateral displacement and base shear corresponding to the yield point of the structure are given in Table 8. The inter-layer displacement angle when the structure yields is shown in Fig. 18.

From Table 8 and Fig. 18, it can be observed that the base shear increases with the height of story, but the difference between the base shear in the X and Y directions of the structure is small. Compared with the X-direction, the Y-direction base shear of the 8-story, 12-story, 16-story, and 20-story models increased by 13.97%, 9.82%, 7.98%, and 7.31%, respectively. When each model yields, the top lateral displacement in X direction is greater than that in Y direction. Compared to the Y-direction, the top lateral displacement in the X-direction of the 8-story, 12-story, 16-story, and 20-story models decreased by 2.38%, 1.69%, 1.16%, and 1.91%, respectively. The difference between the X and Y directions of the model is small, and the influence of the second-order effect of gravity on the two directions is not greatly different. When the structure yields, the maximum inter-layer displacement angles of the 8-story model in both X and Y directions are 1/64. For the 12-story model, the maximum inter-layer displacement angles in the X and Y directions are 1/79 and 1/82, respectively. For the 16-story model, the maximum inter-layer displacement angles in the X and Y directions are 1/82 and 1/83, respectively. For the 20-story model, the maximum inter-layer displacement angles in the X and Y directions are 1/73 and 1/74, respectively. When the structure reaches the yield point, the maximum inter-layer displacement angle in both directions is close, indicating that the structural quality distribution is uniform and the brace arrangement is reasonable.

When the structure yields, the top displacement angles of the 8-story model in X and Y directions are 1/160 and 1/196, respectively, and the change rate is 22.50%. The top displacement angles of the 12-story model in X and Y directions are 1/450 and 1/353, respectively, and the change rate is 21.56%. The top displacement angles of the 16-story model in X and Y directions are 1/505 and 1/388, respectively, and the change rate is 23.17%. The top displacement angles of the 20-story model in X and Y directions are 1/438 and 1/350, respectively, and the change rate is 20.01%. The top inter-layer displacement angle of the 8-story model is the largest, while that of the other models is small. The reason is that when the structure yields, all the braces of the 8-story model appear plastic deformation, while the upper braces of the other models are still in the elastic deformation state.

Table 8
Base shear and top lateral displacement when the structure yields.

Stories	X direction		Y direction	
	Top lateral displacement /mm	Base shear /kN	Top lateral displacement /mm	Base shear /kN
8	278.17	2642.70	284.8	2273.48
12	341.88	3491.32	347.67	3148.52
16	418.50	5304.63	423.37	4881.23
20	551.64	6505.99	562.15	6030.40

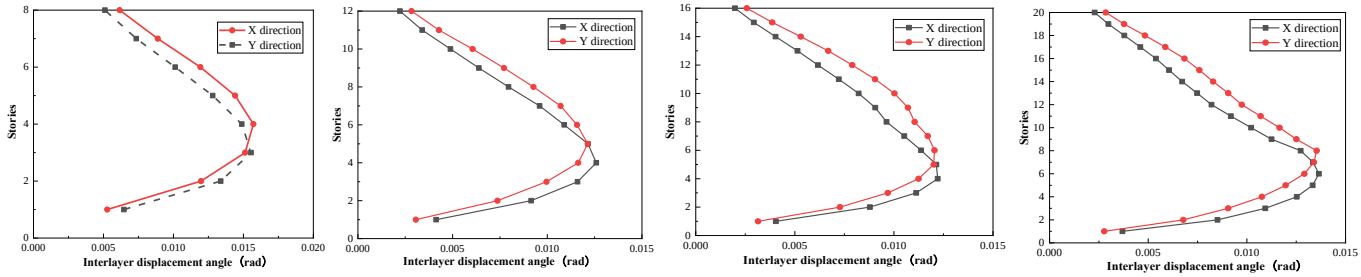

(a) (b) (c) (d)

Fig. 18 Interlayer displacement angle when the structure yields. (a) 8-story. (b) 12-story. (c) 16- story. (d) 20-story

3.6. Determination of performance level

The classification of the performance level of the structure and the determination of its failure state are the key parts of the structural probabilistic seismic capacity analysis. Currently, the main division ideas are based on four performance levels and five failure states. Numerous researchers have conducted quasi-static and shaking table tests on the assembled beam-column joints or frames. Through these tests, the damage development mechanism of the assembled joints is clarified, and the cooperative working ability and damage situation between the joints and other components are understood when applied to the whole frame structure.

In the quasi-static test [27–32], the existing prefabricated beam-column joints did not show the phenomenon of sudden fracture at the joint area or the member, and all of them showed a ductile failure. When the rotation angle of the joint is loaded to 0.02 rad, the specimens are no obviously deformed. When the joint is destroyed, the minimum rotation angle is 0.04 rad and the maximum rotation angle can reach 0.09 rad, showing a good seismic performance. The shaking table test of assembled steel frame structure is less carried out due to its less equipment and limited conditions. Based on the completed shaking table test, the inter-layer displacement angle of assembled steel frame structure [33–35] can reach 1/20 when it is destroyed, which is much higher than the limit of elastic-plastic inter-layer displacement angle of steel frame. Therefore, this paper selects the interlayer displacement angle of 1/25 (when the rotation angle of the joint is 0.04rad) as the collapse critical value of the fabricated steel frame structure for further research.

Referring to the above research content and the Chinese code GB/T 38591-2020 [36], the failure state of the fully bolted assembled steel frame structure is divided into five damage states, and the corresponding four damage limit states are Slight, Moderate, Severe, and Collapse, respectively. The macroscopic description is shown in Table 9.

Table 9
Structural performance level division

Damage states	Beams and columns	Braces	Non-bearing components
No damage	Free from damage	Some slight damage	Some slight damage
Slight damage	Slight deformation occurs at some joints.	Some damage	Less slight damage or some obvious damage
Moderate Damage	Less plastic deformation occurs at the joints.	Less damage	More obvious damage
Severe damage	More beams and columns are severely damaged and there is obvious plastic deformation in the joints.	More damage	Large severe damage
Collapse	More beams and columns are severely damaged	Large damage	More than large severe damages

Note: Some-Less than 10%, Less-10%~30%, more-30%~50%, large-more than 50%.

3.7. Determination of structural performance level limit value

For frame structures with layered properties, the maximum interlayer displacement angle (ISDA) is commonly used to quantify and determine the damage state. The code [37] provides a reference range for the maximum interlayer displacement angle as a quantitative damage index for the damage limit state.

Although the code gives the damage value interval with the maximum inter-layer displacement angle as its index, there are empty intervals and overlaps in each damage value interval. It is not conducive to the subsequent analysis of structural fragility. To address this, the yield displacement angle obtained from the structural pushover curve can be used as the base value and adjusted by multiplying the coefficients of 1, 3, 7, and 10 respectively to obtain the damage values corresponding to different damage states [38]. In this paper, the mean value of the displacement angle in X and Y directions when the structure yields are multiplied by the coefficients to obtain the damage value of the inter-layer displacement angle of each damage state ISDA-1. The ISDA-1 is divided by the structural collapse critical value of 0.04 rad to obtain the structural damage value D1, as shown in Table 10.

Table 10
Performance level damage value interval based on yield displacement angle

Damage states	No damage	Slight damage	Moderate damage	Severe damage	Collapse
ISDA-1	≤ 0.0033	0.0033 ~ 0.0066	0.0066 ~ 0.0132	0.0132 ~ 0.033	≥ 0.033
Damage value D1	≤ 0.08	0.08 ~ 0.25	0.25 ~ 0.58	0.58 ~ 0.83	≥ 0.83

Based on the development of the plastic hinge in structural components, the maximum inter-layer displacement angle (ISDA-2) of the brace, beam, and column in the model are obtained when the damage rate reaches 10%, 30%, and 50%. Similarly, the structural damage value D1 is achieved by dividing ISDA-1 by the structural collapse critical value of 0.04 rad, as shown in Fig. 19.

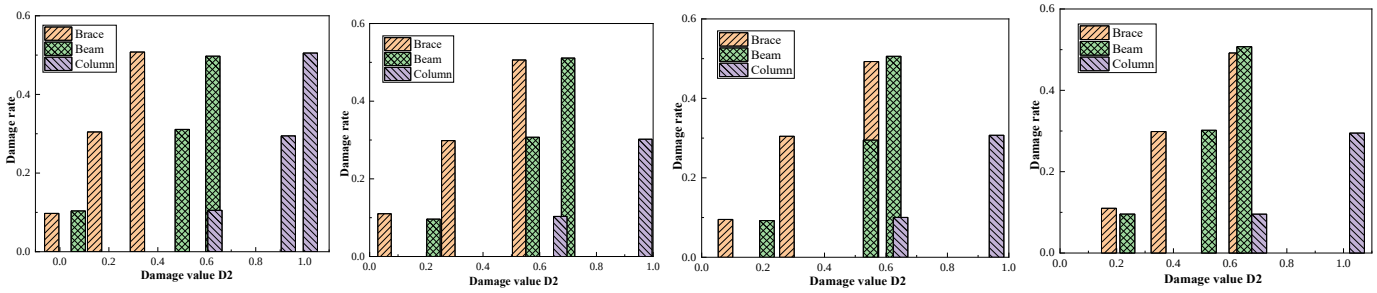

Fig. 19 Damage value distribution. (a) 8-story. (b) 12-story. (c) 16- story. (d) 20-story

From Fig.19, it can be seen that the development trend of the component damage rate in each model is similar. The brace is first damaged and then rapidly reaches 50% damage rate. The development time of the beam and column from 10% damage rate to 30% damage rate is longer, while the beam and column will soon enter the 50% damage rate stage after reaching the 30% damage rate. When the damage rate of the column is 30%, the beam has reached half of the damage probability. Furthermore, when the damage rate of the column reaches 50%, the maximum inter-layer displacement angle is higher than the collapse limit of 0.04 rad, which further reflects the capability design idea of "strong column and weak beam". Combined with the performance level of structural divided above, the 10% damage rate of the brace, 10% damage rate of the beam, 30% damage rate of the beam and 30% damage rate of the column are proposed as the limits of structural performance level, as shown in Table 11.

Table 11
Performance level damage value interval based on component damage rate.

Damage states	No damage	Slight damage	Moderate damage	Severe damage	Collapse
ISDA-2	≤ 0.004	0.004 ~ 0.0085	0.0085 ~ 0.023	0.023 ~ 0.0330	≥ 0.035
Damage value D2	≤ 0.10	0.10 ~ 0.21	0.21~0.58	0.58 ~ 0.88	≥ 0.88

To better improve the damage value of the assembled steel frame for the based-on performance design, referring to the structural damage value interval obtained by the existing researchers on the fragility of steel structures, and taking into account the analysis of the yield displacement angle and the damage rate of the components, The table 9 and Fig.20 presented in this section shows the range of damage values corresponding to each performance level.

Table 12
Definition of damage value range of the frame

Damage states	No damage	Slight damage	Moderate Damage	Severe damage	Collapse
Damage value	0 ~ 0.10	0.10 ~ 0.25	0.25 ~ 0.60	0.60 ~ 0.85	≥ 0.85

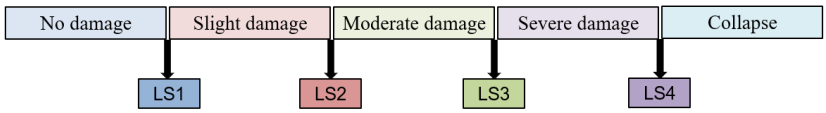

Fig. 20 Frame structure performance levels and corresponding damage states

4. Structural incremental dynamic analysis

4.1. Seismic demand parameters

The peak ground velocity (PGV) is selected as the ground motion intensity parameter (IM). Seismic demand indicators mainly include the strength, stiffness, deformation, and energy consumption etc. Among these indicators, the inter-layer displacement angle (IDSA) is the most widely used. IDSA is used as the overall damage index of the structure, and the single-parameter damage model is established. However, the structure will have cumulative damage under load, and the single-parameter damage model cannot take into account the impact of cumulative energy consumption on the seismic resistance of the structure. Therefore, this paper uses the single-parameter damage model based on the maximum interlayer displacement angle and the two-parameter damage model based on the interlayer displacement angle and energy dissipation to evaluate the seismic performance of the structure.

The single-parameter damage model based on interlayer displacement angle is shown in Eq. (5).

$$D_{\theta} = \frac{\delta_D}{\delta_C} \tag{5}$$

In this equation, δ_D represents the structure's seismic demand, while δ_C represents the structure's seismic capacity. For the purposes of this paper, δ_C is assumed to be 0.04.

The single parameter damage model based on energy dissipation is shown in Eq. (6).

$$D_E = \frac{E_D}{E_C} \tag{6}$$

$$E_C = \frac{2\sum_1^n (W_{ab} f_{yb} \theta_c + W_{uz} f_{yz}) F_D}{M C_y D_y} \tag{7}$$

in which E_D is the structure's energy consumption demand; and E_C is the structure's energy dissipation capacity. n is the number of stories of structure. n_b and n_z is the number of beams and braces in each story, respectively. F_D is the story energy dissipation parameter coefficient. θ_c is the cumulative plastic rotation angle, which is taken as 0.23. C_y is the earthquake influence coefficient. D_y is the structural yield displacement.

The two-parameter damage model based on the interlayer displacement angle and energy dissipation, as shown in Eq. (8)

$$D_M = \alpha D_{\theta} + \beta D_E \tag{8}$$

In which α and β express the weight combination coefficient, with α=0.3 and

β=0.7, respectively. [39].

4.2. Ground motion selection and amplitude modulation

The ground motion is random, and it is necessary to select a large number of seismic waves when the IDA is carried out. Generally, 10 to 20 seismic waves can be selected to avoid the randomness of ground motion, making the structural seismic demand analysis more accurate. According to the ground motion selection principle of ATC-63 [40], 15 seismic waves that meet the requirements of epicentral distance and wave velocity range are selected in the PEER ground motion database, as shown in Table 13 and Fig. 21.

Table 13
Ground motion records

Number	Name	Gauging point	Seismic level	PGA(g)
1	San Fernando	LA-Hollywood Stor FF	5.69	0.22
2	Friuli, Italy	8014 Forgaria Cornino	6.50	0.36
3	Westmorland	Westmorland Fire	5.90	0.37
4	Morgan Hill	Gilroy Array #4	6.19	0.22
5	Superstition Hills	EI CentroImp	6.54	0.36
6	Superstition Hills	Poe Road	6.54	0.47
7	Loma Prieta	Gilroy Array #3	6.93	0.56
8	Loma Prieta	Gilroy Array #4	6.93	0.42
9	Landers	Yermo Fire Station	7.28	0.25
10	Northridge	Beverly Hills－Mulhol	6.69	0.44
11	Northridge	Canyon Country-WLC	6.69	0.40
12	Northridge	LA-Hollywood Stor FF	6.69	0.24
13	Kobe, Japan	Shin-Osaka	6.90	0.23
14	Kocali,Turkey	Duzce	7.51	0.32
15	Chi-Chi, Taiwan	CHY101	7.62	0.44

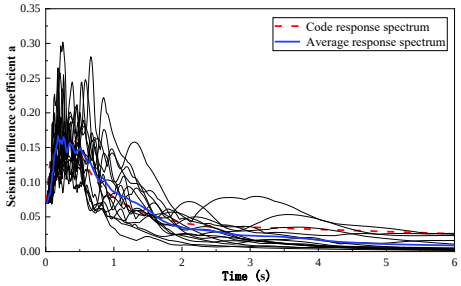

Fig. 21 Seismic wave response spectrum

The average response spectrum values of 15 seismic waves are in good agreement with the standard response spectrum values, which is suitable for structural analysis. The PGA of the selected seismic waves is adjusted to 0.07g, 0.2g, 0.3g, 0.4g, 0.5g, 0.6g, 0.7g, 0.8g, 0.9g, 1.0g, 1.1g, and 1.2g respectively, and IDA is carried out on the high-rise steel frame model with the new fully-bolted core tube beam-column joint.

4.3. IDA results

When the interlayer displacement angle exceeds 0.04 rad, it is considered that the structure has a large plastic deformation and a tendency to collapse. From Fig. 22, it can be observed that the collapse probability of the model decreases with the increase of stories under the action of 8 degrees rare and great earthquakes. Except for the 8-story model, which has a collapse probability of 2/15, the collapse probability of other models is 0 when subjected to the rare earthquakes. The collapse probabilities of the 8-story, 12-story, 16-story, and 20-story models under the action of great earthquakes are 4/15, 3/15, 2/15, and 1/15, respectively. The intensity of the seismic wave S_{CP} is 0.837 g, 0.991 g, 0.976 g, and 1.054 g for the 8-story, 12-story, 16-story, and 20-story models, respectively, when the collapse probability of the structure is 50%. The higher the intensity of the seismic wave S_{CP}, the lower the risk of structural collapse. However, the S_{CP} does not increase with the increase of stories, which is contrary to the fact that the collapse probability decreases with the increase of stories. Therefore, further analysis and judgment are required to determine whether the collapse performance of the structure can be evaluated solely based on the inter-layer displacement angle.

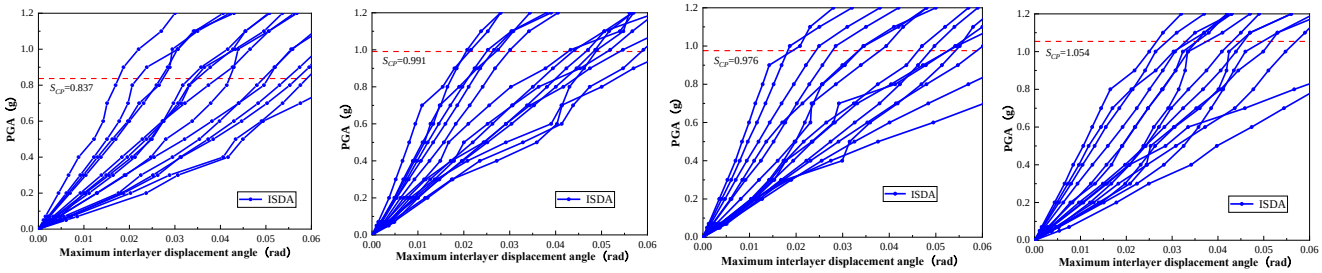

(a) (b) (c) (d)

Fig. 22 IDA results. (a) 8-story. (b) 12-story. (c) 16-story. (d) 20-story

5. Seismic fragility analysis

5.1. Seismic fragility expression

The seismic fragility curve is a plot of the probability of failure as a function of the parameter of the seismic intensity. It can be an objective reflection of the analysis results and is mainly used for the evaluation of the seismic performance of the structures [41]. The structural seismic demand D_E and seismic capacity C_E follow to the normal distribution, and from Eq. (9), the failure probability function P_f is determined:

$$P_f = \Phi\left(\frac{\ln[(e^{a}PGA^{b})/\mu_c]}{\sqrt{\sigma_d^2+\sigma_c^2}}\right) \quad (9)$$

According to the HAZUS specification [42], the $\sqrt{\sigma_s^2+\sigma_c^2}$ value equals to 0.5 when the ground motion parameter is selected as *PGA*; μ_c is the performance level damage limit.

5.2. Seismic demand probability

The relations among the structural seismic demand parameters and the ground motion parameters follow the power exponential function. [43]. To capture this relationship, the logarithm of *PGA* and *D* are determined, respectively, demonstrated in Fig. 23. The IDA results are in regression. Both probabilities for the seismic demand of the structure are given in Table 14.

Table 14
Seismic demand parameters for the structure

Frame	Damage index	Regression equation
8-story	D_θ	$\ln(D_\theta) = 0.8954\ln(PGA) - 0.1799$
	D_G	$\ln(D_c) = 0.8897\ln(PGA) - 0.1481$
12-story	D_θ	$\ln(D_\theta) = 0.9707\ln(PGA) - 0.2636$
	D_G	$\ln(D_c) = 0.9572\ln(PGA) - 0.2439$
16-story	D_θ	$\ln(D_\theta) = 0.9675\ln(PGA) - 0.2855$
	D_G	$\ln(D_c) = 0.9463\ln(PGA) - 0.2524$
20-story	D_θ	$\ln(D_\theta) = 0.9187\ln(PGA) - 0.3091$
	D_G	$\ln(D_c) = 0.8889\ln(PGA) - 0.2875$

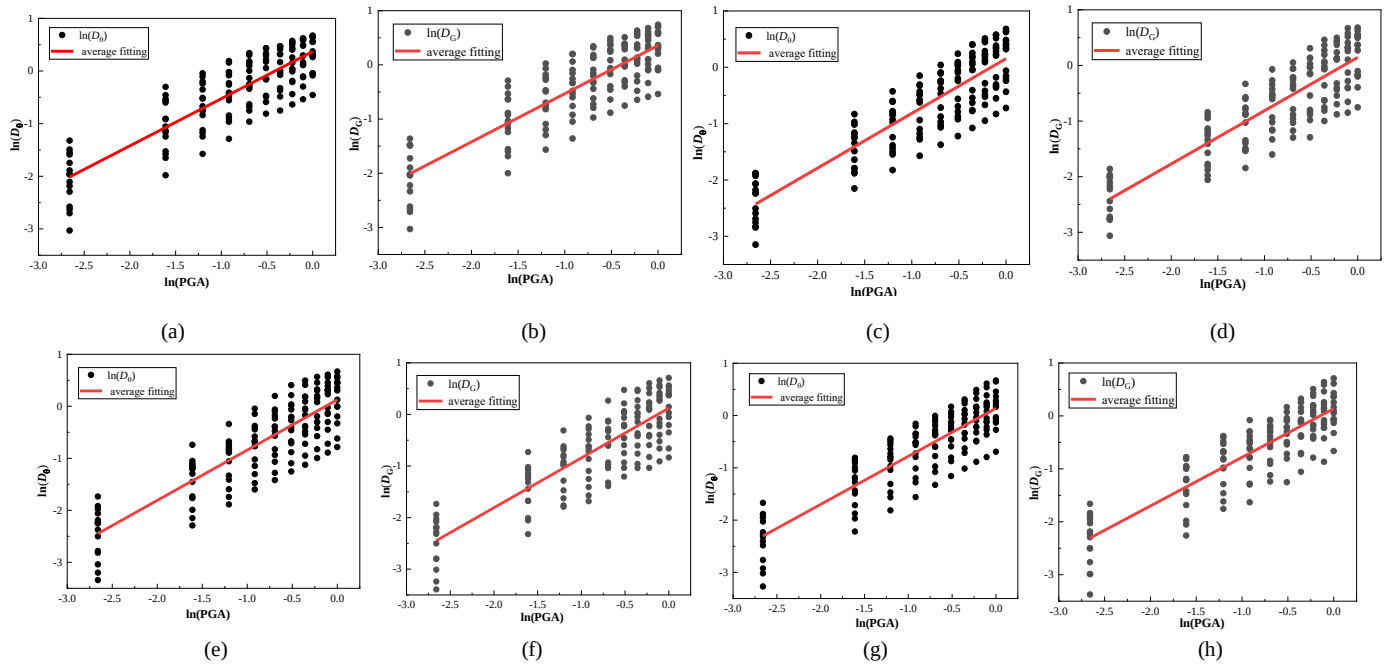

Fig. 23 Steel frame structures regression analysis. (a) 8-story model D_θ. (b) 8-story model D_G. (c) 12-story model D_θ. (d) 12-story model D_G. (e) 16-story model D_θ. (f) 16-story model D_G. (g) 20-story model D_θ. (h) 20-story model D_G

5.3. Seismic fragility analysis

By substituting Eq. (5) to (8) into Eq. (9), the fragility expressions of the structure based on D_θ and D_G can be obtained respectively. The resulting fragility curves are shown in Fig. 24. Considering the unit conversion, the peak acceleration corresponding to the 8-degree rare earthquake and the 8-degree great earthquake is 0.408g and 0.633g, respectively.

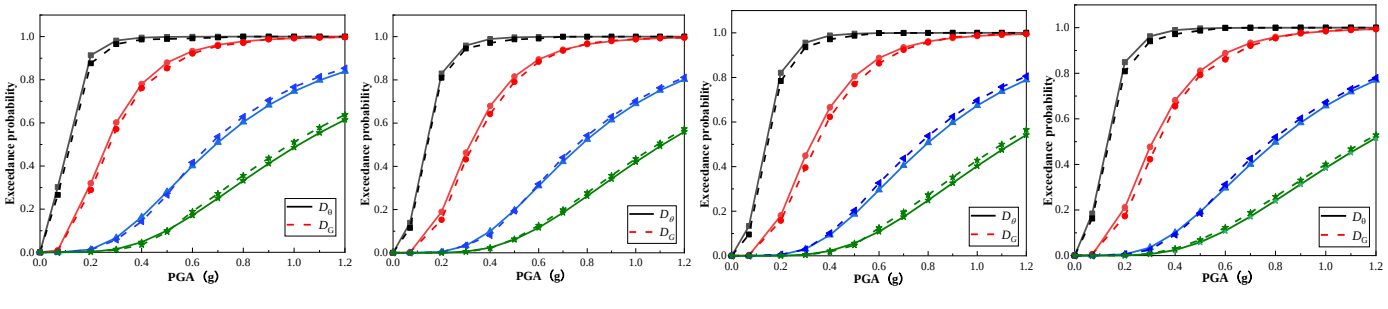

Fig. 24 Fragility curve comparison. (a) 8-story. (b) 12-story. (c) 16-story. (d) 20-story

From Fig. 24, the change trend of the fragility curve according to the single-and two-parameter damage index is similar. When using D_θ as the seismic demand index, during 8-degree rare earthquake, the probability of each model exceeding the LS1 and LS2 limit states is greater than 65%, the probability of exceeding the LS3 limit state is between 10% and 20%, and the probability of exceeding the LS4 limit state is less than 5%. Under the action of 8-degree great earthquake, the probability of each model exceeding the LS3 limit state is between 32% and 44%, while the probability of exceeding the LS4 limit state is about 15%, except that the 8-story model reaches 23.63%. This suggests that the structure may be in a moderate damage state under the action of rare earthquakes, and may be in a severe damage state with the possibility of collapse under the action of great earthquakes.

When taking D_G as the seismic demand index, during 8-degree rare earthquake, the probability of each model exceeding the LS1 and LS2 limit states is greater than 60%, the probability of exceeding the LS3 limit state is between 10% and 15%, and the probability of exceeding the LS4 limit state is less than 5%. Under the action of 8-degree great earthquake, the probability of each model exceeding the LS3 limit state is between 34% and 45%, and the probability of exceeding the LS4 limit state is range from 15% to 25. The model will have a moderate damage state under the action of rare earthquakes, and at the most it will be in a severe damage state. Moreover, the possibility of collapse of the structure under the action of a great earthquake increases.

Regardless of whether D_θ or D_G is used as the seismic demand index. The effect of the number of stories on the probability of structural failure decreases as more stories are added. When the structure is in the limit state of LS3 and LS4, the exceedance probability according to the two-parameter damage index is lower than that according to the single-parameter damage index under the action of the small earthquake peak acceleration. Under the action of the large earthquake peak acceleration, the exceedance probability according to the two-parameter damage index is higher than that according to the single-parameter damage index. It shows that the influence of cumulative damage on the evaluation of structural performance cannot be ignored, especially at the stage of large deformation of the structure. Simply using the maximum inter-layer displacement angle as the damage index will ignore the damage due to plastic deformation of the structure.

6. Analysis of seismic collapse resistance of structure

Although the fragility analysis can provide the structure's collapse probability during the earthquake, it is crucial to evaluate the structure's collapse resistance considering the impact of ground motion and structural uncertainty. The evaluation method of structural performance according to the collapse margin ratio (*CMR*) through the nonlinear time history analysis of the structure during the earthquake, after considering the influence of the uncertainty coefficient β_{TOT} and the spectral shape factor *SSF* on the *CMR*, the adjusted collapse margin ratio (*ACMR*) is obtained. The *ACMR* is used to judge whether the collapse resistance of the structure meets the demand and evaluate whether the structure meets the collapse performance requirement.

The *CMR* is often used to describe the relationship between the fortification demand of structure and the collapse resistance, also known as the structural collapse reserve coefficient, see Eq. (10).

$$CMR = \frac{S_{CP}}{S_{MT}} \tag{10}$$

where S_{CT} is the spectral acceleration corresponding to median collapse capacity, S_{MT} is the spectral acceleration of the rare earthquake and the great earthquake.

Since many factors affect the structural collapse resistance, including the dimension of structural member, structural ductility, and structural effect coefficients, resulting that the *CMR* cannot adequately reflect the structural collapse resistance. The collapse resistance of the structure is highly sensitive to the spectral characteristics of the ground motion. In order to ensure the rationality and accuracy of the structural collapse performance evaluation, the spectral shape factor *SSF* is introduced to adjust the *CMR*. The expression of the *ACMR* is Eq. (11)

$$ACMR = \alpha \times SSF \times CMR \tag{11}$$

in which, α is the model coefficient, and the planar and spatial models take 1.0 and 1.2, respectively.

$$SSF = \exp[\beta_1(\overline{\varepsilon_0}(T) - \varepsilon(T_1))] \tag{12}$$

where β_1 is the spectrum characteristic influence coefficient; $\overline{\varepsilon_0}(T)$ is the spectral shape expectation value, taking as 1.45 in this paper; $\varepsilon(T_1)$ is the value of the spectral shape character, when $T_1 < 0.5$, $\varepsilon(T_1) = 0.6$, when $T_1 > 1.5$ 时, $\varepsilon(T_1) = 0$; when $0.5 \le T_1 \le 1.5$, $\varepsilon(T_1) = 0.6 \times (1.5 - T)$.

The spectrum characteristic influence coefficient can be determined by Eq. (13) and Eq. (14)

$$\mu_c = \frac{\Delta_u}{\Delta_y} \tag{13}$$

$$\beta_1 = 0.17 \times (\mu_0 - 1)^{0.33} \tag{14}$$

where Δ_u is the structural ultimate displacement; Δ_y is the structural yield displacement; μ_0 is the structural effective ductility, when $\mu_c < 8$, $\mu_0 = \mu_c$, and when $\mu_c > 8$, $\mu_0 = 8$.

The models in this paper are all spatial models, so the model coefficient α is 1.2. The *ACMR* of each model is shown in Table 15. The *ACMR* of the model increases with the increase of the structural stories under the 8-degree rare and great earthquake. When the structure is subjected to the rare and great earthquakes, the average *ACMR* of the model is 3.67 and 2.37, respectively.

Table 15
The average *ACMR* of the structures

Stories	$\varepsilon(T_1)$	β_1	*SSF*	*ACMR*	
				Rare earthquake	Great earthquake
8	0.24	0.1719	1.231	3.03	1.95
12	0	0.1898	1.317	3.81	2.45
16	0	0.1823	1.303	3.82	2.46
20	0	0.1807	1.299	4.02	2.60
			Average	3.67	2.37

Since there are some differences between the numerical model and the actual structure, the differences are due to the uncertainty of the structure itself. And the *ACMR* of the structure still does not consider this problem. To make the evaluation results more accurate, the FEMA [44] considers various uncertainties and proposes the structural uncertainty coefficient β_{TOT} to evaluate the degree of agreement between the numerical model and the actual structure. The numerical model is divided into four categories: excellent, good, general, and very poor. Then, the allowable values of *ACMR* under different collapse probabilities are given according to the structural uncertainty coefficient β_{TOT}.

The allowable collapse probability of the structure under rare earthquakes is 10% (*ACMR*10%) according to the FEMA evaluation criteria for structural collapse resistance. In general, each group of structures should meet this requirement. However, since the collapse probability of some single structures may exceed this limit, the collapse probability of a single structure should not exceed 20% (*ACMR*20%). Based on this, in view of the uncertainty of the structure, the allowable value of the average *ACMR* for each group of structures is *ACMR*10%, that is, $\overline{ACMR_i} \ge ACMR10\%$. The allowable value of the *ACMR* for a single structure is *ACMR*20%, that is, $ACMR_i \ge ACMR20\%$. If the structure meets the above two evaluation criteria, the steel frame with the new fully-bolted core tube beam-column joint is considered to have good seismic performance and collapse resistance. According to the above analysis,

the analysis results of the simplified mechanical model of the new fully-bolted core tube beam-column joints adopted in this paper are consistent with the experimental data, but there are still some differences. And the actual deformation of the new joints is not fully considered by the simplified mechanical model. The numerical model also does not fully consider the connection structure between the actual floor slabs and brace and the main component, so the quality of the numerical model is defined as general. According to the results of static elastic-plastic analysis, the four models designed in this paper have the ductile failure mode of "strong column and weak beam", which meets the seismic fortification requirements of the specification and reflects the idea of "structural capacity design". Therefore, the structural design quality is at a good level. Considering the influence of the reduced scale effect of the previous test joints, there is a certain gap with the actual structure. Thus, the quality of the structural and component test data is identified as good.

Based on the above analysis, the allowable *ACMR* value of the new fully-bolted core tube joint steel frame after considering the structural uncertainty is shown in Table 16.

Table 16
Structure ACMR allowable value

Structure and component test data quality	Good
Structure design quality	Good
Numerical model quality	General
β_{TOT}	0.75
*ACMR*5%	3.43
*ACMR*10%	2.61
*ACMR*15%	2.18
*ACMR*20%	1.88
*ACMR*25%	1.66

Note: *ACMR*5% is the structural collapse margin ratio when the collapse probability is 5%, and so on.

Combined with Table 15 and Table 16, the collapse resistance of the new fully bolted steel frame is evaluated. Under the action of rare earthquakes, the average *ACMR* of the model is 3.67, which is greater than the *ACMR*10% allowable value of 2.61, that is, it meets the $\overline{ACMR_i} \geq ACMR10\%$. The *ACMR* values of each model are greater than the *ACMR*20% allowable value of 1.88, which satisfies the $ACMR_i \geq ACMR20\%$. The test results show that the steel frame with the new joint is capable of withstanding rare earthquakes as required by code [45].

Under the action of great earthquakes, the average *ACMR* value of the steel frame model is 2.37, which is between the allowable values of *ACMR*10% and *ACMR*20%, it does not meet the evaluation requirements. However, the *ACMR* values of each model are greater than the *ACMR*20% allowable value, which satisfies the $ACMR_i \geq ACMR20\%$. The *ACMR* value of the 8-story model is the smallest. This may be due to the relatively strict seismic measures for the high-rise structures and relatively loose seismic measures for the low-rise or multi-story structures in the code of China. Therefore, when the new joint is applied to the actual project, some seismic strengthening measures should be taken to ensure that the safety reserve for the collapse resistance of the new fully-bolted assembled joint steel frame structure under the action of great earthquake is sufficient. In conclusion, the new joints are suitable for the multi-story and high-rise steel frame structures, and the steel frame with the new joint in this paper meets the seismic fortification requirements of the code.

7. Conclusions

The models for multi-story and high-rise steel frames with new joints have been identified, and the static elastic-plastic time-history analysis was carried out to confirm the rationality of the support arrangement and the applicability of the new joints. After defining the damage value under each damage state, the seismic fragility and collapse resistance of the steel frame models with new joint of different stories were analyzed. The main conclusions can be summarized as follows.

(1) The steel frame structure with new fully-bolted core tube beam-column joint meets the requirements of seismic fortification under the frequent and rare earthquakes. The maximum inter-layer displacement angle in both directions is close, indicating that the mass distribution of the structure is uniform, and the brace arrangement in this paper is reasonable.

(2) The plastic hinge development order of each model is brace-beam-column. When the inter-layer displacement angle of the structure reaches 0.02 rad, most of the braces and beams of each model have plastic hinges, and some of the middle columns in the bottom story enter the plastic deformation stage, indicating that each model conforms to the idea of "capacity design". The new joints are suitable for multi-story and high-rise buildings with the proper component selection and arrangement.

(3) The performance level of the assembled steel frame structure is re-divided. Based on the structural yield displacement angle and the component damage probability, the damage value interval of the new joint steel frame structure is determined to be [0.1, 0.85].

(4) Under the 8-degree rare earthquakes, the steel frame structure with new fully-bolted core tube beam-column joint may be in the severe damage stage at most, while under the 8-degree great earthquakes, the steel frame with new fully-bolted core tube beam-column joint may collapse. This emphasizes the significance of considering cumulative damage during the evaluation of structural performance, particularly in the large deformation stage.

(5) The *ACMR* values of the steel frame structure with new fully-bolted core tube beam-column joint meet the evaluation criteria under the rare earthquakes, However, under the great earthquakes, the *ACMR* values do not meet the evaluation criteria. Therefore, in practical engineering, certain seismic strengthening measures should be taken to make the structure have sufficient safety of collapse resistant under the great earthquakes.

Acknowledgment

This study was financially supported by the National Natural Science Foundation of China (Grant No.52268029) and the Basic Research Project of Science and Technology Department of Sichuan Province (Grant no. 2023JDZH0035) and Natural Science Foundation of Sichuan Province (Grant No. 2023NSFSC0381).

References

[1] D. Miller. Lessons learned from the Northridge earthquake. Engineering Structures, 1998, 20 (4): 249-260.
[2] M. Nakashima, K. Inoue, M. Tada. Classification of damage to steel buildings observed in the 1995 Hyogoken-Nanbu earthquake. Engineering Structures, 1998, 20 (4): 271-281.
[3] E.P. Popov, T.S. Yang, S.P. Chang. Design of steel MRF connections before and after 1994 Northridge earthquake. Engineering Structures, 1998, 20 (12): 1030-1038.
[4] Shahidi F, Rezaeian A, Jamal-Omidi M, et al. Investigation of the ConXL moment connection cyclic behavior in box columns without filling concrete with different arrangement of collar bolts[J]. The Structural Design of Tall and Special Buildings, 2015, 24(5): 317-350.
[5] Lee S, Park J, Shon S, et al. Seismic performance evaluation of the ceiling-bracket-type modular joint with various bracket parameters[J]. Journal of Constructional Steel Research, 2018, 150: 298-325.
[6] Y. Wang, Q.Q. Ma, Y.T. Yang, X.L. Liu. Research on mechanical properties of H-shaped steel beam-steel tube column joints of assembled steel structure [J]. Progress of building steel structure, 2019, 21 (03): 13-22.
[7] Hosseini S M, Rahnavard R. Numerical study of steel rigid collar connection affecting cyclic loading[J]. Engineering Structures, 2020, 208: 110314.
[8] X.C. Liu, A.X. Xu, A.L. Zhang, et al. Static and seismic experiment for welded joints in modularized prefabricated steel structure. Journal of Constructional Steel Research, 2015, 112: 183-195.
[9] X.C. Liu, S.H. Pu, A.L. Zhang, et al. Static and seismic experiment for bolted-welded joint in modularized prefabricated steel structure. Journal of Constructional Steel Research, 2015, 115: 417-433.
[10] X.C. Liu, Z.W. Yang, H.X. Wang, et al. Seismic performance of H-section beam to HSS column connection in prefabricated structures. Journal of Constructional Steel Research, 2017, 138: 1-16.
[11] X.L. LU, N.F. SU, Y. ZHOU. IDA-based seis-mic fragility analysis of a complex high-rise structure[J]. Journal of Ertha quake Engineering and Engineering Vibration,2012,32(5):19-25.
[12] Fanaie N, Ezzatshoar S. Studying the seismic behavior of gate braced frames by incremental dynamic analysis (IDA) [J]. Journal of Constructional Steel Research,2014,99:111-120.
[13] Mohebi B, Chegini T A H, Miri T A R. A new damage index for steel MRFs based on incremental dynamic analysis[J]. Journal of Constructional Steel Research,2019,156:137–154.
[14] M.S. Pandikkadavath, K.M. Shaijal, S. Mangalathu, et al. Seismic robustness assessment of steel moment resisting frames employing material uncertainty incorporated incremental dynamic analysis. Journal of Constructional Steel Research, 2022, 191: 107200.
[15] W. Wang, S.L. Hu, C. Zou. Seismic fragility analysis of beam-through braced steel frames based on incremental dynamic analysis [J]. Journal of Building Structures, 2021,42 (04): 42-49.
[16] B. Li, Z. Cai, Z. Duan. Selection of hazard-consistent ground motions for risk-based analyses of structures[J]. Structural Safety, 2023, 104: 102365.
[17] D.A. Kiureghian. Analysis of structural reliability under parameter uncertainties. Probabilistic Engineering Mechanics, 2008, 23(4): 351-358.
[18] X.L. Lv, N.F. Su, Y. Zhou. IDA-based seismic fragility analysis of a complex high-rise structure. Earthquake Engineering and Engineering, 2012, 32(5): 19-25. (in Chinese)
[19] N. Fanaie, S. Ezzatshoar. Studying the seismic behavior of gate braced frames by incremental dynamic analysis (IDA). Journal of Constructional Steel Research, 2014, 99: 111-120.
[20] B. Mohebi. A new damage index for steel MRFs based on incremental dynamic analysis. Journal of Constructional Steel Research, 2019, 156: 137-154.
[21] Y.P. Chu, Y. Zhong, P. Luo, et al. Experimental study on the seismic performance of the

new fully-bolted beam-column joint[J]. Journal of Constructional Steel Research, 2022, 199: 107619.
[22] R. Bjorhovde, A. Colson, J. Brozzetti. Classification system for Beam-to-column Connections. Journal of Structural Engineering, ASCE, 1990,116(11):3059-3076.
[23] Eurocode 3: Design of Steel Structures: Part 1.1 General Rules and Rules for Building, CEN, Bruxelles: Commission of the European Communities, 1993.
[24] GB50017-2017. Standard for design of steel structures. Beijing: China Architecture & Building Press, 2017. (in Chinese)
[25] W.X. Yang. Structural influence coefficient of Y-shaped eccentrically braced steel frames. Shanghai Jiao Tong University, 2011. (in Chinese)
[26] ATC, Seismic Evaluation and Retrofit of Concrete Buildings, ReportNo. ATC-40[S]. Applied Technology Council: Redwood City, California, 1996.
[27] Y.X. Zhang, M.Y. Cheng, A.L. Zhang, et al. Research on the mechanical performance of box column integral core barrel type full bolt connection. Journal of Building Structures, 2020,41 (05): 180-189. (in Chinese)
[28] Y.X. Zhang, X.D. Wang, X. Zhao, et al. Comparative study on performance test of box-type plunger welding and one-way bolt core-cylinder connection joints. 2021, 38 (10): 103-118. (in Chinese)
[29] A.L. Zhang, Z.P. Guo, X.C. Liu, et al. Experimental study on seismic performance of assembled steel frame joints with Z-shaped cantilever beam segment splicing. Engineering Mechanics, 2017,34 (08): 31-41. (in Chinese)
[30] X.C. Liu, M.L. Chen, X.S. Chen. Research on seismic behavior of assembled steel beam-to-column joints with diagonal braces. // Tianjin University, Tianjin Steel Structure Association. (in Chinese)
[31] A.L. Zhang, L. Su, Z.L. Cao, et al. Experimental study on seismic performance and finite element analysis of Z-type fully bolted beam-to-column connections with double-sided connections. Industrial Building, 2021,51 (02): 59-65+89. (in Chinese)
[32] W. Wang, Y.S. Chen, Y.Y. Chen, et al. Experimental study on full-scale shaking table test of layered assembly support steel frame with external PC composite wall panel. Journal of Building Structures, 2019, 40 (02): 88-97. (in Chinese)
[33] Y.S. Chen, W. Wang, Y.Y. Chen. Vibration table test of three-story full-scale layered assembled braced steel frame structure. Journal of Building Structures, 2018,39 (09): 22-29. (in Chinese)
[34] Y.X. Zhang, X.T. Cheng, A.L. Zhang, et al. Shaking table test study on autoclaved aerated concrete wall panels for steel frame steel tube anchor slip joints. Progress in building steel structure, 2021,23 (10): 67-74. (in Chinese)
[35] GB / T 38591-2020 Standard for seismic resilience assessment of buildings [S]. Beijing: China Standard Press, 2021. (in Chinese)
[36] GB50011-2010 Code for seismic design of buildings [S]. Beijing: China Construction Industry Press, 2001. (in Chinese)
[37] G. Li, G.D. Cheng. Performance-based seismic design of structures-theory, method and application [M]. Science Press, 2004.
[38] Q. Xu, S.S. Zhen, Y.Z. Han, et al. Study on seismic fragility of steel frames based on global damage index. Vibration and impact, 2014,33 (11): 78-82. (in Chinese)
[39] ATC-63. Quantification of building seismic performance factors [R].
[40] ATC-63 Project Report (90% Draft), FEMA P695/April 2008.
[41] Y. Pan, Y.L. Bao, Y.X. Liu, Seismic fragility analysis of base-isolation structure connected with large span special-shaped steel corridor. China civil engineering Journal, 2021, 54(2): 20-29. (in Chinese)
[42] HAZUS 99 user's manual: Federal Emergency Management Agency[M]. Washington, D.C., 1999.
[43] C.A. Cornell, F. Jalayer, R.O. Hamburger, et al. Probabilistic basis for 2000 SAC federal emergency management agency steel moment frame guidelines. Journal of structural engineering, 2002, 128(4): 526-533.
[44] Federal Emergency Management Agency. NEHRP provisions for the Seismic Rehabilitation of Buildings[M]. Report FEMA 273 (Guidelines) and 274 (Commentary), Washington, D.C., 1997:144-198.
[45] FEMA, Quantification of building seismic performance factors, FEMA P695, Federal Emergency Management Agency, Washington, DC, June 2009.